RESEARCH ARTICLE

A double-rotor MOF gaining benchmark rotational dynamics at extreme cold temperatures: correlated motion and regulation by CO_2

Jacopo Perego,[a] Charl X. Bezuindehout,[a] Silvia Bracco,[a] Giacomo Prando,[b] Luciano Marchio',[c] Mattia Negroni,[a] Piero Carretta,[b] Angiolina Comotti,* [a] and Piero Sozzani*[a]

[a] Dr. J. Perego, Dr. C. X. Bezuidenhout, Prof. S. Bracco, Prof. L. Marchio', Dr. M. Negroni, Prof. A. Comotti, Prof. P. Sozzani
Department of Materials Science
University of Milano Bicocca
Via R. Cozzi 55, Milano, Italy
E-mail: piero.sozzani@unimib.it
[b] Dr. G. Prando, Prof. P. Carretta
Department of Physics
University of Pavia
Via Bassi, 6 – 27100 Pavia, Italy
[c] Prof. L. Marchio'
Dipartmento di Scienze Chimiche, della Vita e della Sostenibilità Ambientale
Università degli studi di Parma
Parco Area delle Scienze 17/a, Parma, Italy

Supporting information for this article is given via a link at the end of the document.

Abstract: The implementation of sophisticated rotor dynamics in solids belongs to the efforts to minimize the activation energy for rotation, thus achieving fast yet controllable and correlated motion to construct switches and motors. Our endeavour was to realize two rotors operating in the same MOF architecture capable of supporting fast motional regimes, even at extremely cold temperatures. 4,4'-bipyridine (bipy) and bicyclo[1.1.1]pentanedicarboxylate (BCP) ligands, coordinated to Zn clusters, fabricated a pillar-and-layer 3D array of orthogonal rotors. The bipy rings display sophisticated rotary dynamics concerted with the framework, which swings between two equivalent arrangements in a dynamically disordered structure. Upon lowering temperature, the framework undergoes a crystallographic disorder-to-order phase-transition, which, in turn, enabled hyper-fast mobility of the second rotor (BCP) following a cascade mechanism. Variable temperature XRD, ^{2}H solid-echo and ^{1}H T_1 relaxation NMR collected down to 2 K, revealed the rapid rotary mechanics and energy barriers of rotation as low as 24 cal/mol, a real benchmark for complex arrays of rotors. These rotors explored multiple con-rotary and dis-rotary modes switched-on/off and modulated by the thermal energy, as singled out by DFT modelling. Additionally, an external stimulus of CO_2 diffused to interaction sites through the open pores, dramatically changed the sensitive rotor dynamics. Collectively, the intriguing gymnastics of multiple rotors, devised cooperatively and integrated into the same framework, gave the opportunity to engineer hyper-mobile rotors (10^7 Hz at 4 K) in MOF crystals.

Introduction

The mechanics of motion in solids has been attracting increasing interest from the perspective of designing organized molecular rotors, motors and machines, the goal being to control their functions and properties, such as the commutation of light into mechanical work, dielectric and optical properties and ferroelectricity.[1] Different strategies have been addressed for the targeted construction of dynamic materials, including the use of self-assembly principles, host-guest compounds and hybrid materials.[2]

The exploitation of low density and porous materials has been stimulating, since they provide adequate free volume for molecular group rotation and act as platforms for switching and modulation by absorption from the gas phase.[3] The exquisite engineering of barriers to group-revolution in the solid-state, down to the energy limit of a few small calories per mole, ensured continuous rotation, even at a few kelvins.[4]

Within the realm of porous materials, MOFs are outstanding for their synthetic versatility and the opportunity they provide to design modular structures, while preserving crystalline order and periodicity.[5] Moreover, MOFs have been shown to support localized dynamics without disrupting the primary architecture. For this reason, MOFs were successfully employed to insert rotors in the frameworks as ligands bridging the metal ions or cluster nodes.[6]

The project to assemble distinct fast rotors within a single framework of structural complexity, without disrupting their mobility, is attractive for realizing a synergistic smart organization of multiple dynamic elements. Pillared-MOFs offer this opportunity being composed by two juxtaposed ligands, which can be designed as molecular rotors. Additionally, due to their structural flexibility and tunability, they did show superior properties and have been successfully proposed for reversible gas-capture and water sorption from the air.[7]

In the present work we engineered a bi-component MOF built by two distinct ultrafast and interacting molecular rotors of diverse chemical nature and symmetry (saturated vs. unsaturated moieties and twofold vs. threefold symmetry), organized as layers and pillars forming a porous 3D architecture. They displayed a benchmark mobility even at the extremely cold temperature of 2 K, and cooperated in a concerted motion. In turn, rotary motion could change its rate and mechanism either by the chemical stimulus of CO_2 entering the pores or by a thermally

triggered order-disorder phase transition. Specifically, 2D sheets comprising BCP rotors are interpenetrated by bipyridine pillars in a multi-dynamical building, wherein the rotors experience sequential motional behaviour. The dynamics of bipy pillaring rotors were coupled with framework dynamics through a hydrogen-bonded network, switching at low temperature to the ordered state, which consequently triggers the hyper-fast motion of BCP in the 2D sheets. The intriguing interplay of BCP rotors generates a sophisticated arrangement of geared and anti-geared rotator relationship in a cascade relaxation phenomenon, with co-rotating and counter-rotating configurations. DFT computations help define the energy states for the rotational configurations, which explore an attractive flat-energy landscape, achieving the intensely pursued goal of collective unhindered continuous rotation in solid matter. In fact, the lowest energy rotational configuration explores extreme mobility of 10^7 Hz at 4K with an exceptionally low activation energy of 0.024 kcal/mol. Motional trajectories and energy barriers were derived from ^{2}H solid-echo NMR and ^{1}H T_1 relaxation-times, depicting multiple profiles and specifically, in the restricted 2K-10K range, a unique full-excursion rotor relaxation profile, at which most molecular dynamics are quenched.

Within this variegated scenario of extreme mobility, CO_2 could intervene from the gas phase in a sophisticated manner, tuning the two rotors at the same time. The rotors were proved accessible to the gas molecules entering the porous crystals, as shown by adsorption isotherms and gas adsorption coupled to microcalorimetry. CO_2 inclusion dramatically affected the structure, mechanism, speed and activation energy of the rotators, as measured by ^{2}H line-shape and ^{1}H relaxation NMR. Remarkably, *in situ* PXRD studies demonstrated CO_2 induced ordering of the framework coordinated with rotor dynamics upon pressure increase,.

Results and Discussion

The pillared double-rotor MOF was synthesized by self-assembly of two distinct molecular rotors (BCP = bicyclo[1.1.1]pentane-1,3-dicarboxylate; bipy = 4,4'-bipyridine) and Zn ions under solvothermal conditions at 85°C in DMF/MeOH mixture. The highly crystalline powder was filtered and washed with fresh solvent (SI). Activation under a high vacuum at 140°C effectively removed guest molecules, generating permanent porosity and providing excess free volume that could sustain fast rotational motion and dynamics in the solid state (named FTR-P1 Pillared Free Trigonal Rotor). Infrared spectroscopy showed a shift of the C-O stretching band from 1664 to 1596 cm^{-1} which signifies the coordination of BCP carboxylate groups to Zn ions. ^{13}C and ^{1}H MAS NMR demonstrated the purity of the samples and complete guest removal. TGA showed the robustness of the compound up to 330°C. The open porosity of samples was proven by CO_2 adsorption isotherms at 195 K yielding a maximum adsorbed amount of 1.7 mmol/g (about 4 molecules per unit cell), which corresponded to the filling of the accessible free volume estimated by the crystal structure (Figure S10).

Order and disorder in the crystal structure. The activated material was subject to variable temperature XRD, both as single crystals and powders. Single-crystal XRD data collection was performed between 275 K and 110 K. The crystal structure is formed by two independent and interpenetrated 3D networks. The 3D networks consist of 2D sheets comprising BCP carboxylate ligands coordinated to the Zn cations in a paddle wheel fashion, forming a rhombic geometry (Figure 1), which are pillared by bipy ligands, generating the 3D framework with **pcu** topology.[8] The interpenetrated crystal structure exhibits 1D open channels running parallel to the *c* axis, which are decorated by the bipyridine aromatic units. The channel cross-section ranges from 4.7×5.2 Å^2 to 2.7 x 1.7 Å^2, confirming the generation of an ultra-microposours material. The aromatic rings of bipy units can be differentiated into distinct moieties; one is exposed to the empty cavities (ring A) while the other is situated within the rhombous of the 2D layers (ring B) (Figure 1D).

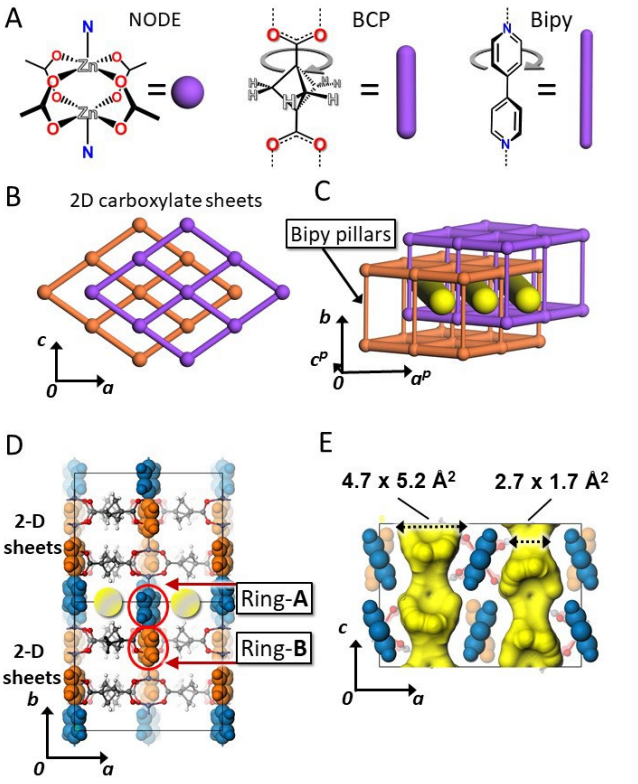

Figure 1. A) Zn-paddlewheel node, molecular structures of BCP and bipy linkers. B) 2D sheets made by BCP dicarboxylate linkers and Zn nodes forming a rhombic shape. C) Two interpenetrated networks (highlighted in violet and orange colors) forming channel-like cavities. D) Crystal structure highlighting the ring A facing the channel and ring B in the 2D layer highlighted in blue and orange, respectively. E) Open channels and ring A highlighted in yellow and blue, respectively.

The crystal structure at high temperature exhibited extensive disorder on both bipy and BCP ligands, suggesting the presence of distinct rotors. The crystal structure (space group *Cmma*) shows 2D disordered sheets due to two symmetry-related locations of the main BCP-axis (50% occupancy) shifted parallel to one another (Figure 2A). This disorder can be generated by a rotation of the paddle-wheel node around its axial coordination axis. The pillaring bipy ligand displays orientational disorder of its aromatic rings over 2-sites with a symmetry site-occupancy of 50%. Additionally, the bipyridine rings exposed to empty cavities

(ring A) forms C–H ··· O interactions with the disordered carboxylate oxygen atoms of the other network (Figure S13: D···A distance = 3.42 Å, D-H···A angle of 170.4°). The rotation of the paddle-wheel weakens the C–H ··· O interactions and prompts the rotation of ring A and or vice-versa, generating a 'gymnastics' between the bipy ring A and the metal-carboxylate 2D layer (Figure 2A). At 160 K an ordered phase of lower symmetry (space group *Pmma*) is formed corresponding to either of the disordered networks present in the high-temperature structure (Figure 2B). Furthermore, a diffused electron density describing a toroidal shape about the main molecular axis of BCP and corresponding to CH_2 moieties is observed: a preliminary indication for the presence of flat energy profiles explored by the methylene crown (Figure 2D). Consequently, the disorder in both ligands suggests the presence of two types of rotators (bipy and BCP) in the crystalline porous architecture.

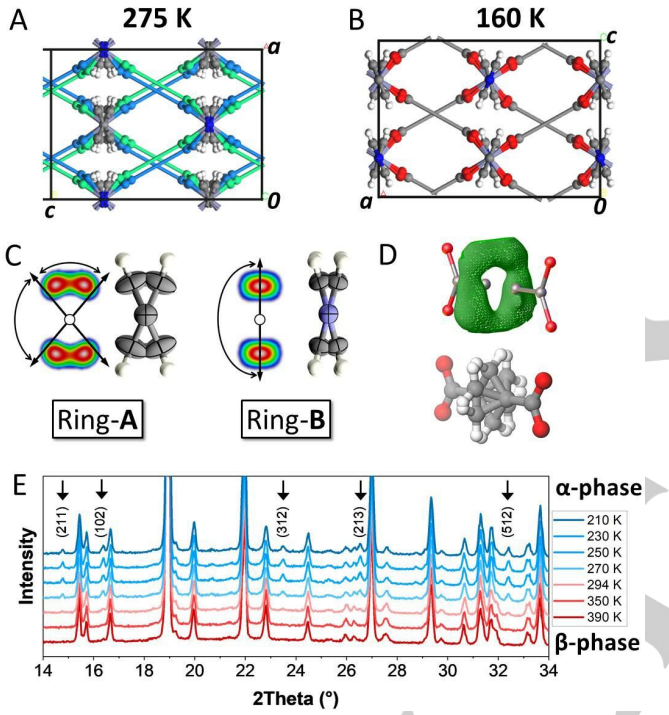

Figure 2. Crystal structures of FTR-P1 with A) symmetry related BCP dicarboxylated axis (β-phase, blue and green rods) and B) ordered BCP axis (α-phase, grey rods). C) Diffused electron density and thermal ellipsoids with 80% probability of bipy rings as viewed along the main rotation axis. D) Diffused electron density with a toroidal shape about the main BCP axis, showing the dynamics of the BCP rotor. E) VT-PXRD patterns as function of temperature showing the transition from the low temperature to high temperature phase. New distinct PXRD peaks appear in the α-phase as indicated by the Miller indices.

The phase transformation from the low temperature phase (denoted α-phase) to high temperature phase (β-phase) could be followed accurately by varable temperature powder X-ray diffraction patterns (VT-PXRD). Diffractograms collected between 210 K and 390 K show the progressive appearence of a few peaks upon cooling (Figure 2E). The profiles were processed by two-phase Rietveld refinement and interpreted as the contribution of two independent structures with distinct relative ratios. It is worth noting the occurrence of the transition from the ordered (α-phase) to the disordered phase (β-phase) on increasing temperature, as reported in Figure 2E.

Bipy rotor dynamics. Solid state NMR spectroscopy gives an insight into the dynamics of materials: in particular, spin-lattice relaxation times (T_1) and ^{2}H NMR are among the most informative methods for discovering molecular rotors and their motional properties such as the rotational frequencies, associated energies and mechanism of motion.[9] To infer these properties, we synthesized an analogous MOF with BCP and perdeuterated bipyridine (FTR-P1d) to selectively study the dynamics of bypiridine molecules by ^{2}H spin-echo NMR. FTR-P1d exhibits virtually the same properties, as indicated by PXRD trace and CO_2 isotherm (Figure S11 and S17). Variable temperature ^{2}H solid-echo NMR spectroscopy, implemented by lineshape analysis, allowed us to follow the intriguing reorientational dynamics of bipyridine rings (Figure 3A-F).[10]

Indeed, it was possible to interpret the complex modulation of the line-shapes as the summation of contributions of the two distinct phases and the two independent A and B rings. The β-phase is the main contributor in the high temperature spectra (293 K – 390 K): the rings facing the channels (ring A) experience fast reorentational jumps (about $5*10^6$ Hz) among 4 conformational minima with a 4-site jump mechanism. The 4-site reorientational angles of ±39.5° and ±140.5° are precisely dictated from the profile simulation of the spectra at each recording temperature (Figure 3A). These ring jump-angles match the SC-XRD observations (Figure 2C). The 4-site jump mechanism comprises breaking and reforming of the C–H···O interactions coupled with the rotational dynamics of the paddle-wheel.

The ring B, which resides within the 2D layer, essentially underwent a fast 180° flip reorientation coupled with ±28° jumps, accounting for the shrinking of the profile at high temperatures. In the spectra below 210 K, the more ordered α-phase prevails, as highlighted by the emergence of two singularities separated by 124.7 kHz width due to a fully static arrangement of confined ring B within the NMR time scale (< 10^3 Hz). However, the ring A which is exposed to the channels experiences only a fast 2-site 180° flip reorientation and no 4-site reorentations. The 4-site reorientation mechanism can only be supported by rotational dynamics of the paddle-wheels, which become ordered at temperatures below 210 K. The simulation profiles of two selected spectra containing the distinct components are shown in Figure 3B and 3D.

These sophisticated dynamics are strongly modulated by temperature, changing both the α– vs β–phase content ratio (Figure 3 G) and reorentation frequencies of each phase (Figure 3 A and F). In particular, upon lowering the temperature, the ring A in the β-phase shows restricted motion, progressively reducing the 4-site mechanism and favouring simple oscillations of ±39.5°, but still maintaining fast frequencies of 10^8 Hz. Conversely, in the α-phase, ring A maintains its 180° flip reorientation with a frequency of $4*10^6$ Hz, even at temperature a low as 150 K. Interestingly, in the α-phase, the differentiation between the two bipy rings reaches an extreme: highly mobile rotor (ring A) and a static ring (ring B) are observed, whilst both rotors are mobile in the β-phase.

From the deconvoluted profiles, the α and β-phase ratios as depicted in the diagram of Figure 3G: the maximum rate of change for the transition is observed at 220 K. This transition from the ordered to the disordered phase with increasing

temperature mirrors the DSC trace which shows an endotherm with a maximum at 220 K (ΔH=21-23 J/g) (Figure 3H).

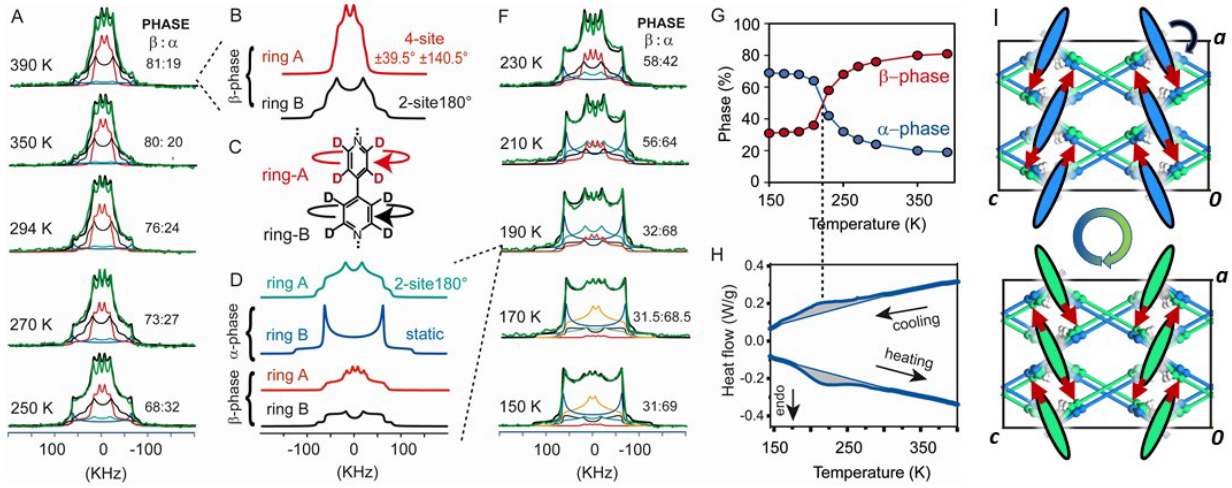

Figure 3. ^{2}H NMR spectra of FTR-P1d: A) from 250 K to 390 K and F) from 150 K to 230 K. Deconvoluted components of ^{2}H NMR spectra at 390 K (B) and 190 K (D). C) Molecular structure of perdeuterated-bipy showing the aromatic rings A and B. G) Quantification of α- and β-phase from the deconvoluted ^{2}H NMR spectra. H) DSC traces exhibiting the transition from the ordered to the disordered phase. I) Bipy ring A arrays viewed along the main rotational axis (blue and green pales) alternatively coordinated with the blue and green frame.

Low rotational energy barriers of 1.2 and 2.0 kcal/mol were estimated for rotor A, exposed to the channels, in the β- and α-phases, respectively. Rotator B exhibits a higher barrier of 3.9 kcal/mol in the β-phase and a "static" arrangement ($k < 10^3$ Hz) in the α-phase (Figure S25). Additionally, ^{2}H NMR results show further modulation of the bipy dynamics due to the degree of order in the framework (the ratio of the α- and β-phases), although the mobility of rotator A persisted at low temperature even in the ordered α-phase. By applying the Eyring equation, we can extract the entropy change from the ground to the excited state. Rotator A in the disordered β-phase shows a negative value of -26 cal mol^{-1} K^{-1} and a rotational frequency at infinite temperature $K_0 = 3*10^7$ Hz, which is much lower than that expected from the inertial mass of a single rotator ($2*10^{12}$ Hz):[11] therefore, cooperative reorientation must be invoked. Essentially, the pillaring bipy rotors operate collectively in a concerted manner with neighbouring rotors and the framework. These dynamics facilitate the breaking and reformation of the C–H···O interactions between the two networks as ring A reorientates (Figure 3I).

BCP rotor dynamics down to 2 K. Owing to the aforementioned diffused electron density of the BCP CH_2 groups, the presence of fast molecular rotatory dynamics are expected (Figure 4). Variable temperature ^{1}H T_1 relaxation times of BCP hydrogens was extremely informative regarding the exceptional mobility of BCP rotors, which could not even be quenched at a low temperature of 2 K. The ^{1}H T_1 measurements of BCP hydrogens was carried out using a MOF sample containing deuterated bipy ligands (FTR-P1d) which eliminates the contribution of the bipy moieties to the ^{1}H spectrum generating a single narrow resonance of BCP methylenes. Thus, ^{1}H T_1 relaxation times would not be affected by signal overlapping and spin-diffusion due to bipy.

The measurements, collected at distinct observation frequencies of 16.56 and 45.86 MHz, are reported in Figure 4 A-D. The relaxation rates plotted as a function of temperature exhibit a complex profile which can be fitted using six Kubo-Tomita (K-T) functions with maxima at 4, 36, 49, 95, 139 and 175 K. Surprisingly, at very low temperatures from 10 K to 1.6 K, it is possible to identify a full K-T profile with a maximum relaxation rate at 4 K, demonstrating an extremely high mobility of the BCP molecules in the 10^7 Hz regime (Figure 4B, expansion at low T). Indeed, the activation energy for this process is as low as 24 cal/mol. The rotor shows a six orders-of-magnitude change in frequency, from 10^3 Hz to 10^8 Hz in the small temperature range of 1 to 7 K, implying that the rotator exhibits a pronounced tendency to thermally activated motion. Such dynamical behaviour at low temperatures is only comparable to that of methyl rotation.[12] Above 10 K, the motional process explores a succession of phenomena with gradually increased activation energies of 445, 688, 940, 1816 and 2947 cal mol^{-1} and correlation times (τ_0) of about 10^{-10} s. These phenomena were interpreted as various configurations of groups of neighbouring rotators with relative rotational directions, co-rotating or counter-rotating. Since individual BCP rotators cannot be differentiated in the unit cell, we resort to accounting for intermolecular interactions among rotators during their rotation. We built a model considering an ensemble of eight vicinal rotators as arranged within the crystal structure (Figure 4E,F).

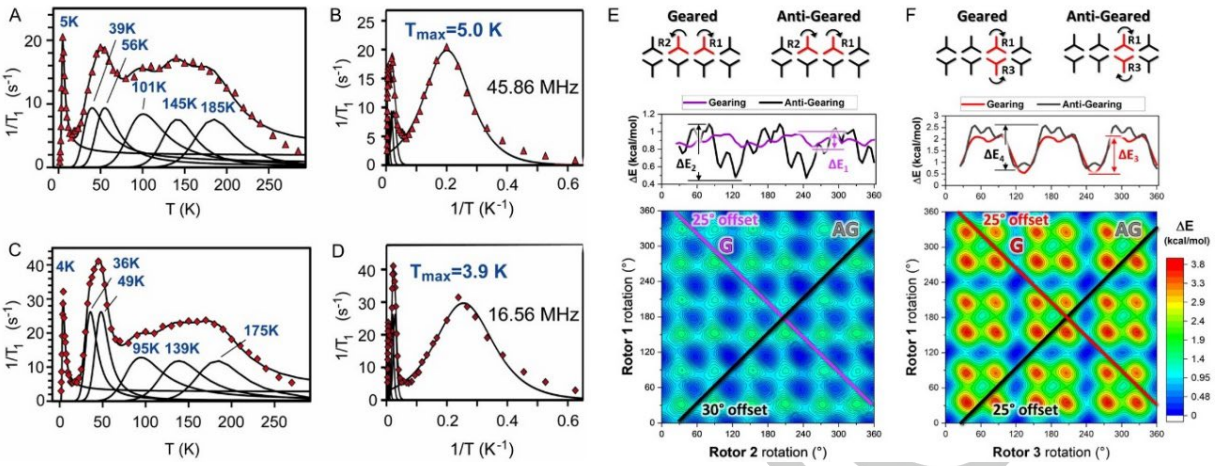

Figure 4. ^{1}H relaxation rates as function of temperature (A,C) and reciprocal of temperature (B,D) at two distinct magnetic fields. E) and F) The 2D DFT scans for two side-by-side rotors (E) and two crossed rotors (F). Top: graphical illustration of the model indicating the geared and anti-geared rotations with the curved arrows. Middle: The ΔE plot for the most optimal gearing and anti-gearing rotations. Bottom: The 2D contour map with the rotation of rotors pairs R1 and R2 (E) and R1 and R3 (F) on the X- and Y-axes with the colours indicating the ΔE. The colour scale ranges from 0 kcal/mol (blue) to 3.8 kcal/mol (red). The lines indicate the most optimal Gearing (G) and Anti-gearing (AG) pathways on the energy surfaces, with the relative rotor rotational offset indicated for each.

DFT modeling. DFT calculations of the energy profiles were determined for rotor-couples (rotators 1-2 and 1-3) employing a 2-D potential energy scan of both rotors in the pair (Figures S27 and S28). Each rotor was scanned about its rotation-axis, and the interaction with surrounding BCP units was taken into account. The energy barrier for single rotor rotations was identified to be 0.9-1.0 kcal/mol and therefore cannot generate lower barriers. The potential energy contour map for a couple of side-by-side rotors, R1 and R2, allowed us to identify the preferential paths comprising the reciprocal motion of the two rotors, yielding the lowest activation barriers (Figure 4E). The purple line with 45° negative inclination indicates the synchronous clockwise and counter-clockwise rotation of the two rotors at the same speed. A geared motion with an offset of 25° between the two rotators exemplifies the lowest energy pathway with a 70 cal/mol energy barrier. Various mechanisms-of-motion with higher barriers can be explored following different paths on the energy surface, such as the anti-geared mechanism, indicated by the black line (45° positive inclination), with an energy barrier of 310 cal/mol and an offset of 30°.

The simultaneous rotation of the crossed rotators, R1 and R3 (Figure 4F), produces higher barriers of 750 cal/mol and 925 cal/mol for the geared and anti-geared mechanisms, respectively. The rotors have more kinetic energy at higher temperatures to explore the rotational energy landscape, thus exploring several other paths that entail higher rotational energy barriers (Figure S29). Consequently, the calculated geared and anti-geared rotational barriers for rotors in different configurations perfectly explain the series of experimental energy barriers measured from ^{1}H T_1 relaxation times. Remarkably, the lowest energy barrier at very low temperature is generated by the synchronized geared motion of side-by-side rotators.

Rotor modulation by CO_2. We explored the CO_2 adsorption capability of the MOF at variable temperature (273 K – 298 K) and up to 1 bar: FTR-P1d reaches 83% of the full loading at 273 K (Figure 5). The isotherms follow a Langmuir profile and yield an isosteric heat of adsorption of 32.5 kJ/mol from the IAST method. Independently, we performed a volumetric sorption experiment with direct *in-situ* microcalorimetric measurements of the heat released during CO_2 absorption (for the methodology refer to SI).[13]. The experiment was performed at 293 K up to 1 bar, obtaining a heat of adsorption of 32.4 kJ/mol, which validates the isotherm derived from the isosteric heat of adsorption. Notably, the CO_2 isotherm profile perfectly matches the cumulative heat profile for the adsorption process (Figure 5B): i.e. the cumulative heat of adsorption (Q) increases linearly with CO_2 loading (N). This suggests that the enthalpy of adsorption would remain virtually constant over a wide pressure range and is ascribed to the microporous nature of MOF. In fact, the constricted 1D channels are progressively occupied site-after-site and CO_2 molecules in each site display interactions exclusively with pore walls at the expense of CO_2-CO_2 interactions. The matrix-CO_2 interaction energy, as evaluated by PW-DFT calculations, is E_{int}=32.7 kJ/mol, consistently with the above reported experimental values.

To further study the MOF-CO_2 structural relationship, variable pressure PXRD (VP-PXRD, at 293 K) and variable temperature PXRD (VT-PXRD, under 1 bar CO_2) experiments were conducted. Both experiments unveiled a framework structural change, from the β-phase to the α'-phase (FTR-1-d·$x$$CO_2$), upon sufficient accumulation of CO_2 into the channels. A pressure-induced structural change to the α'-phase occurs under mild conditions with an onset pressure of 0.4 bar CO_2 at RT (Figure 5D). This ordering effect on the overall architecture is the structural counterpart of the NMR measurements, highlighting the reduced freedom of bipy rotors induced by CO_2 molecules. The CO_2 loaded crystal structure, produced by Rietveld refinement of the PXRD pattern at 253 K, establish

that each CO_2 molecule in the channel is surrounded by two bipy rings (ring A) and four BCP ligands. The CO_2 molecules are disordered over two equivalent crystallographic positions, tilted by an angle of about 34° with respect to the channel-axis and arranged parallel to the bipy rings at a short $Ring_{centroid}\cdots C_{CO2}$ distance of 3.87 Å (Figure 5E). Upon desorbing CO_2, the crystal structure revers back to the original disordered β-form.

In this scenario, we further highlight, by frequency-sensitive methods, how CO_2 interactions with both rotors affect their dynamics in the 10^3 -10^9 Hz frequency regime. ^2H solid echo NMR spectra of the FTR-P1d sample under 3 bars of CO_2 as a function of temperature (Figure 5F) showed a drastic reduction in rotational frequencies of bipy rings compared to those occurring at the same temperature in the empty FTR-P1d. Additionally, the mechanism can be finely modulated by CO_2 inclusion: for ring-A (facing the channels) jumps of ±39.5° dominate over the whole temperature range, demonstrating its restricted dynamics. Consequently, 4-site reorientation and 2-site 180° flips are reduced and increase the activation energy to 5.2-5.3 kcal/mol owing to the protrusion of the rings temporarily into the channels, now occupied by CO_2 molecules. This represents a penalty paid by the rotators A of 3.5 kcal/mol with respect to the empty sample.

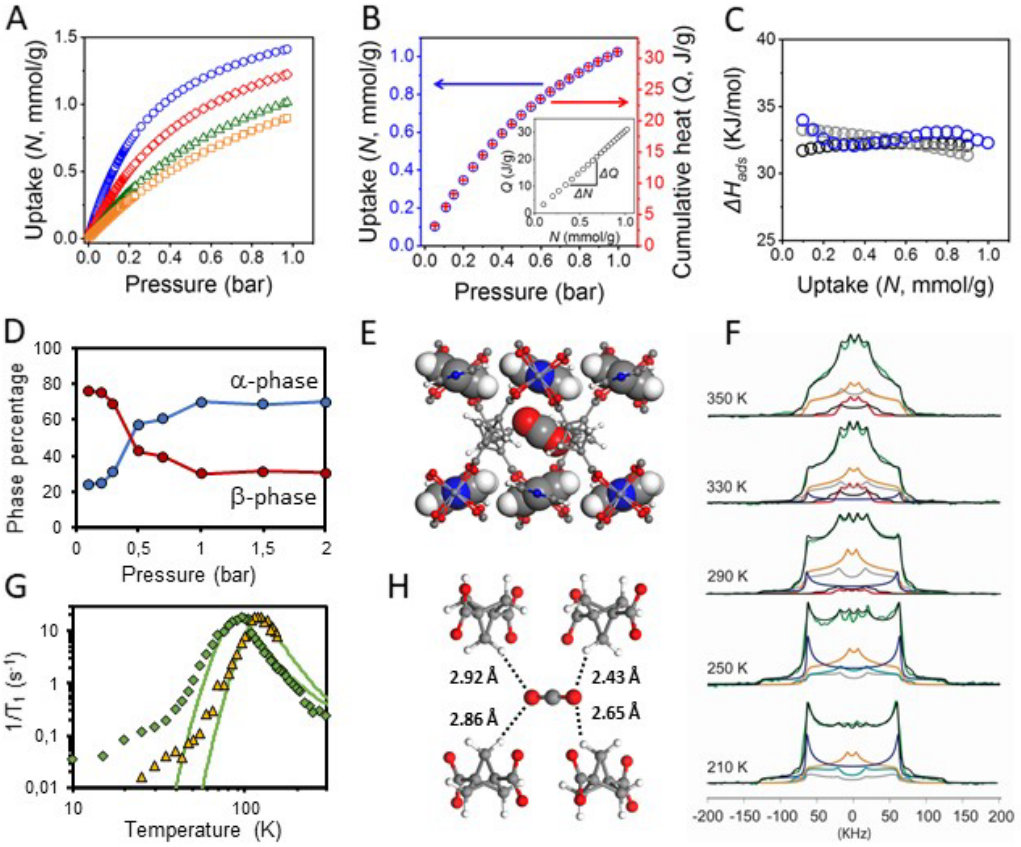

Figure 5. A) CO_2 adsorption isothems at 273, 283, 293 and 298 K (blue,red, orange, green and yellow circles, respectively). B) CO_2 loading (N) at 293 K and cumulative heat (Q) released on increasing loading with increasing the pressure. The inset shows a plot *Q* vs *N* with the gradient indicated. C) Isosteric heat of adsorption by IAST method from isotherms fitting with Langmuir equation (grey circles) and Langmuir-Freundlich equation (light blue circles) compared to heat released from direct measurement at 293 K and increasing pressur (blue circles). D) Phase percentage at 293 K and on increasing loading up to 2 bar. E) Crystal structure of FTR-P1d loaded with CO_2 at 253 K and 1 bar: an individual CO_2 molecule sitting in the pocket. F) ^2H NMR spectra of FTR-P1d laoded with CO_2 (3 bar) as function of temperature (black line). The total simulated profile is highlighted in green. The deconvoluted line-shapes for each rotational mechanism are the following: 4-site ±39.5°/ ±140.5° reorientation for ring A in the β-phase (red line), 2 site 180° and 180°/±28° reorientation for ring B in the β-phase (gray and black lines, respectively), 2 site 180° reorientation for ring A in the α-phase (light blue line), static pattern for ring B in the α-phase (blue line) and 180°±39.5° jumps for ring A in both phases (yellow line).G) ^1H T_1 relaxation times of BCP at 45.86 Hz of FTR-P1d loaded with CO_2 (3 bar). H) A single CO_2 molecule confined in the pocket, highlighting the interaction with BCP moieties

Furthermore, a dramatic change in the ^1H T_1 measurements for BCP rotors occurs, showing suppression of multiple phenomena observed in the empty sample. The dynamic behaviour is simplified, and the relaxation pattern can be fitted by two K-T equations (peak temperatures at 95 K and 125 K). The latter indicates two motional phenomena with derived energy barriers of 1.2 and 1.8 kcal/mol and correlation times (τ_0) of about $1.8*10^{-11}$ s and $8.8*10^{-12}$ s, respectively (Figure 5G). Therefore, the interaction of CO_2 with the BCP rotors dominates their rotational energy landscape since CO_2 forms short C–H···O contacts with all the rotors, as highlighted in the crystal structure of the loaded sample (Figure 5H). Molecular Mechanics calculations, using CO_2 loaded FTR-P1 under periodic boundary conditions, confirm the increase in activation energy for all rotational phenomena previously observed at lower activation energies in the empty compound (SI). These results clearly demonstrate the ease of manipulating the dynamics of two distinct rotors by an external stimulus due to the porosity of MOF which enables diffused-in molecules to act directly on the rotators.

Conclusions

Two arrays of fast rotors were engineered in the crystalline structures of pillared MOFs, FTR-P1 and its deuterated analogue FTR-P1d. The assembly of fast molecular rotors generates a sophisticated dynamical scenario due to the interplay of distinct mechanical behaviour and diverse motional regimes. The rotors operate in spatiotemporal succession, covering a temperature range from 390 K down to 2 K, with a multiple *pyrotechnic* motional evolution, while exploring systematically ultrafast dynamics (large amplitude jumps, coordinative oscillations, multiple gearing and anti-gearing rotation).

The discovery by PXRD and solid-echo ^2H NMR of a disorder-to-order phase transition explains the intriguing framework-rotor modulation: above the phase transition (β-phase), bipy rotors are correlated to the framework dynamics in a collective swinging dance while, below the phase-transition (α-phase), bipy rings experience individual rapid 180° flip rotation in the static framework. At low-temperature the BCP rotor undergoes fast rotation by running over smooth energy landscape: single and multiple coordinated geared/anti-geared rotations are switched-on in succession, as they explore discrete energy levels. Strikingly, a hyperfast geared mechanism, with an energy barrier as low as 24 calories per mole, was excited at temperatures between 1.6 and 10 K, showing the potential of the low-density crystals for converting the very low thermal-energy into rotary motion.

The active manipulation from external chemical stimuli, such as CO_2, easily delivered from the gas phase onto the porous FTR-P1 crystals, induced a disorder to order transition on lowering temperature, which in turn tuned bipy motional mechanism. As for BCP rotors, CO_2 entering the nano-channels changed and simplified the activation energy landscape, resulting in the manipulation of the dynamical picture, as photographed by spin-lattice ^1H NMR relaxations,.

The achievement of a complex molecular system in a crystal underlines the utility of crystal engineering to suggest ways for dosing the right amount of order and disorder of multiple rotators in a single architecture. These achievements are expected to be of interest for providing a platform for fine-tuned devices useful in applications such as active materials in sensing, radiation manipulation and molecular switching.

Acknowledgements

The Ministero dell'Istruzione, dell'Università e della Ricerca for MIUR-Progetto Dipartimento di Eccellenza 2018-2022 and PRIN 20173L7W8K (NEMO) are acknowledged for the financial support.

Keywords: Crystal Engineering • Metal Organic Framework • • Molecular Rotors • CO_2 capture • NMR Spectroscopy

[1] a) S. Krause, B. L. Feringa, *Nat. Rev. Chem.* **2020**, 4, 550–562. b) Coskun, M. Banaszak, R. D. Astumian, J. F. Stoddart, B. A. Grzybowski, *Chem. Soc. Rev.* **2012**, *41*, 19-30. c) J. Michl, E. Charles, H. Sykes, *ACS Nano* **2009**, *3*, 1042-1048. d) F. Castiglioni, W. Danowski, J. Perego, F. King-Chi Leung, P. Sozzani, S. Bracco, S. J. Wezenberg, A. Comotti, B. L. Feringa, *Nature Chem.* **2020**, *12*, 595-602. e) S. Tavi, A. Kaeser, M. Matsumoto, T. Aida, S. I. Stupp, *Nature Chem.* **2015**, *7*, 281-294. f) B. H. Wilson, C. S. Vojvodin, G. Gholami, L. M. Abdulla, C. A. O'Keefe, R. W. Schurko, S. J. Loeb, *Chem.* **2021**, *7*, 202-211.

[2] a) W. Danowski, F. Castiglioni, A. S. Sardjan, S. Krause, L. Pfeifer, D. Roke, A. Comotti, W. R. Browne, B. L. Feringa, *J. Am. Chem. Soc.* **2020**, *142*, 9048-9056. b) L. Kobr, K. Zhao, Y. Shen, A. Comotti, S. Bracco, R. K. Shoemaker, P. Sozzani, N. A. Clark, J. C. Price, C. T. Rogers, J. Michl, *J. Am. Chem. Soc.* **2012**, *134*, 10122-10131. c) H. Deng, M. A. Olson, J. F. Stoddart, O. M. Yaghi, *Nature Chem.* **2010**, *2*, 439-443. d) S. Bracco, M. Beretta, A. Cattaneo, A. Comotti, A. Falqui, K. Zhao, C. Rogers, P. Sozzani *Angew. Chem. Int. Ed.* **2015**, *54*, 4773–4777. e) A. Comotti, S. Bracco, T. Ben, S. Qiu, P. Sozzani, *Angew. Chem. Int. Ed.* **2014**, *53*, 1043-1047. f) C. S. Vogelsberg, M. A. Garcia-Garibay, *Chem. Soc. Rev.* **2012**, *41*, 1892–1910. g) C. S. Vogelsberg, S. Bracco, M. Beretta, A. Comotti, P. Sozzani, M. A. Garcia- Garibay, *J. Phys. Chem. B* **2012**, *116*, 1623-1632. h) S. Bracco, A. Comotti, P. Valsesia, B. F. Chmelka, P. Sozzani, *Chem. Commun.* **2008**, *39*, 4798-4800.

[3] a) W. Danowski, T. van Leeuwen, S. Abdolahzadeh, D. Roke, W. R Browne, S. J. Wezenberg, B. L. Feringa, *Nature Nanotech.* **2019**, *14*, 488–494. b) P. Martinez-Bulit, A. J. Stirk, S. J. Loeb, *Trends Chem.* **2019**, *1*, 588–600. c) S. Bracco, A. Comotti, P. Sozzani, *Acc. Chem. Res.* **2016**, *49*, 1701-1710. d) S. Horike, R. Matsuda, D. Tanaka, S. Matsubara, M. Mizuno, K. Endo, S. Kitagawa, *Angew. Chem. Int. Ed.* **2006**, *45*, 7226–7230. e) S. K. Elsaidi, M. H. Mohamed, C. M. Simon, E. Braun, T. Pham, K. A. Forrest, W. Xu, D. Banerjee, B. Space, M. J. Zaworotko, P. K. Thallapally, *Chem. Sci.* **2017**, *8*, 2373-2380. f) A. Comotti, S. Bracco, P. Valsesia, M. Beretta, P. Sozzani, *Angew. Chem. Int. Ed.* **2010**, *49*, 1760-1764. g) S. Bracco, T. Miyano, M. Negroni, L. Marchio', P. Sozzani, N. Tohnai, A. Comotti, *Chem. Comm.* **2017**, *53*, 7776-7779. h) J. Seo, R. Matsuda, H. Sakamoto, C. Bonneau, S. Kitagawa, *J. Am. Chem. Soc.* **2009**, *131*, 12792-12800.

[4] J. Perego, S. Bracco, M. Negroni, C. X. Bezuidenhout, G. Prando, P. Caretta, A. Comotti, P. Sozzani, *Nature Chem.* **2020**, *12*, 845-850.

[5] a) H.-C- Zhou, S. Kitagawa, *Chem. Soc. Rev.* **2014**, *43*, 5415-5418. b) H. Lyu, Z. Ji, S. Wuttke, O. M. Yaghi Chem. 2020, 6, 2219-2241.

[6] a) S. Bracco, F. Castiglioni, A. Comotti, S. Galli, M. Negroni, A. Maspero, P. Sozzani, *Chem. Eur. J.* **2017**, *23*, 11210-11215. b) C. S. Vogelsberg, F. J. Uribe-Romo, A. S. Lipton, S. Yang, K. N. Houk, S. Brown, M. Garcia-Garibay, *Proc. Nat. Acad. Sci.* **2017**, *114*, 13613-13618. c) M. Inukai, T. Fukushima. Y. Hijikata, N. Ogiwara, S. Horike,

S. Kitagawa, *J. Am. Chem. Soc.* **2015**, *137*, 12183-12186. d) Y.-S. Su, E. S. Lamb, I. Liepuoniute, A. Chronister, A. L. Stanton, P. Guzman1, S. Pérez-Estrada, T. Y. Chang, K. N. Houk, M. A. Garcia-Garibay and S. E. Brown, *Nature Chem.* **2020**, *13*, 278–285. e) N. B. Shustova, T.-C. Ong, A. F. Cozzolino, V. K. Michaelis, R. G. Griffin, M. Dinca, *J. Am. Chem. Soc.* **2012**, *134*, 15061-15070.

[7] a) B. Chen, C. Liang, J. Yang, D. S. Contreras, Y. L. Clancy, E. B. Lobkovsky, O. M. Yaghi, S. Dai, *Angew. Chem. Int. Ed.* **2006**, 45, 1390-1393. b) H. Chun, D. N. Dybtsev, H. Kim, K. Kim, *Chem. Eur. J.* **2005**, *11*, 3521-3529. c) A. Bajpai, M. Lusi, M. J. Zaworotko, *Chem. Commun.* **2017**, *53*, 3978-3981. d) P. Nugent, Y. Balmabkhout, S. D. Burd, A. J. Cairns, R. Luebke, K. Forrest, S. Ma, B. Space, L. Waoitas, M. Eddaoudi, M. J. Zaworotko, *Nature* **2013**, *495*, 80-84. e) J. Seo, R. Matsuda, H. Sakamoto, C. Bonneau, S. Kitagawa *J. Am. Chem. Soc.* **2009**, *131*, 12792-12800.

[8] V. Guillerm, K. Dongwook, J. F. Eubank, R. Luebke, X. Liu, K. Adil, M. S. Lah, M. Eddaoudi, *Chem. Soc. Rev.* **2014**, *43*, 6141-6172.

[9] A. Abragam in *Principles of Nuclear Magnetism*, Oxford University Press, Oxford, **2011**.

[10] a) J. H. Kristensen, G. L. Hoatson, R. L. Vold, *Solid State Nucl. Magn.Reson.* **1998**, *13*, 1-37. b) A. Comotti, S. Bracco, A. Yamamoto, M. Beretta, T. Hirukawa, N. Tohnai, M. Miyata, P. Sozzani, *J. Am. Chem. Soc.* **2014**, *136*, 618-621.

[11] Owen, N. L. in *Internal Rotation in Molecules, Ch. 6* (Ed.: W. J. Orville-Thomas), Wiley, **1974**.

[12] a) J. Nakagawa, M. Hayashi, *J. Chem. Phys.* **1984**, *80*, 5922-5925. b) V. Ilyushin, et al. *J. Mol Spectrosc.* **2011**, *267*, 186-190. c) K. D. Hensel, M. C. L. Gerry, *J. Chem. Soc. Faraday Trans.* **1994**, *90*, 3023-3027.

[13] a) W. K. Feldmann, K.-A. White, C. X. Bezuidenhout, V. J. Smith, C. Esterhuysen, L. J. Barbour, *ChemSusChem,* **2020**, *13*, 102-105. b) J. Perego, C. X. Bezuidenhout, A. Pedrini, S. Bracco, M. Negroni, A. Comotti, P. Sozzani, *J. Mater Chem A* **2020**, *8*, 11406-11413.

Entry for the Table of Contents

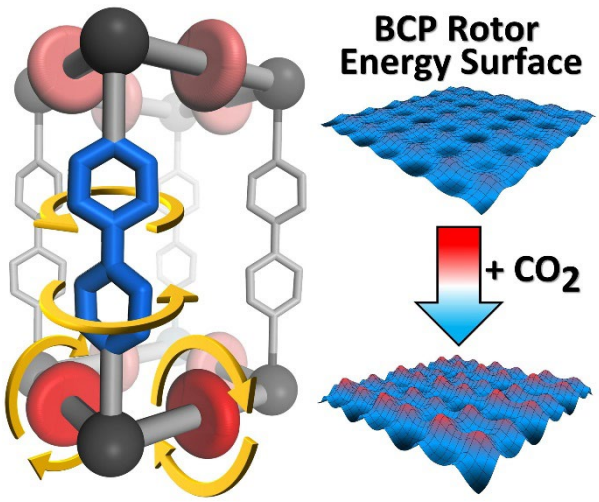

Two rotors engineered in a MOF architecture exhibit multiple dynamical phenomena and a concerted motion with the framework. Rotational frequencies are still as high as 10^7 Hz at 4 K due to the virtually flat energy landscape. CO_2 captured in the pores regulates the mechanism and dynamics of the two rotors.